IET Renewable Power Generation

WILEY

IET The Institution of Engineering and Technology

ORIGINAL RESEARCH OPEN ACCESS

Intelligent Power Control in Smart Photovoltaic Systems Using M5-Pruned Decision Tree for Enhanced Grid Voltage Modulation

Khechafi Sofiane[1] | Bouchhida Ouahid[1] | Bouraiou Abdelouahab[1] | Mujammal Ahmed Hasan Mujammal[1] | Mohammed Abdulelah Albasheri[1] | Mohit Bajaj[2,3,4] | Olena Rubanenko[5]

[1]Research Laboratory of Electrical Engineering & Automatic (LREA), University of Dr. Yahia Fares, Medea, Algeria | [2]Department of Electrical Engineering, Graphic Era (Deemed to Be University), Dehradun, India | [3]Hourani Center for Applied Scientific Research, Al-Ahliyya Amman University, Amman, Jordan | [4]College of Engineering, University of Business and Technology, Jeddah, Saudi Arabia | [5]Department of Power Plants and System, Vinnytsia National Technical University, Vinnytsia, Ukraine

Correspondence: Mohit Bajaj (mohitbajajphd@gmail.com) | Olena Rubanenko (olenarubanenko@vntu.edu.ua)

Received: 21 October 2025 | **Revised:** 26 November 2025 | **Accepted:** 17 December 2025

ABSTRACT

This paper presents an advanced and smart enhancement to the direct power control (DPC) strategy using grid voltage modulation for three-phase photovoltaic (PV) inverters. It introduces and evaluates three DC-link voltage control techniques: the proportional-integral (PI) controller, the fuzzy logic controller (FLC), and a novel M5-Pruned (M5P) decision tree–based algorithm. While PI-based DPC remains widely used, it is often constrained by its sensitivity to gain tuning, limited adaptability, suboptimal dynamic response, and not ideal decoupling of active and reactive powers. FLC offers greater flexibility and can handle nonlinearities more effectively, yet it still lacks precise control and structured scalability. To address these limitations, this study proposes the M5P-based control approach, a data-driven, self-adaptive strategy that combines model transparency with the ability to handle complex system behaviour efficiently. Simulation results show that the proposed M5P method significantly reduces total harmonic distortion to 0.20%, outperforming both PI (0.57%) and FLC (0.53%) controllers. Furthermore, it achieves complete decoupling of power components, enhances dynamic stability, and eliminates the need for manual gain tuning. The methodology is validated through extensive simulations in MATLAB/Simulink, highlighting its effectiveness under both steady-state and transient conditions. These results establish the M5P-based controller as a promising candidate for next-generation intelligent PV grid integration systems.

1 | Introduction

The accelerated growth and integration of renewable energy systems, such as photovoltaic (PV) systems, into electrical grids has significantly transformed the landscape of modern power systems [1]. Ensuring high power quality, reliability, and fast dynamic response in these grid-connected systems is a persistent challenge, particularly because of the discontinuous and nonlinear nature of renewable energy generation [2, 3]. Among the various control strategies developed for managing power converters and grid interfaces, direct power control (DPC) has gained considerable attention for its simplicity and dynamic performance [4, 5]. Traditional control techniques, such as proportional-integral (PI) controllers, have been widely used in DPC schemes to regulate essential variables such as grid current, active and reactive powers, and DC-link voltage [6, 7]. Since PI controllers facilitate effortless implementation and tuning, their performance is often limited by system nonlinearities,

parameter variations, and external disturbances [8]. In practical scenarios, the fixed-parameter nature of PI controllers may result in suboptimal transient response, increased overshoot, and reduced robustness, especially under rapidly changing operating conditions [9]. Several studies in the literature have addressed DC-link voltage regulation in grid-connected power converters using conventional control techniques such as PI controllers, sliding-mode control (SMC), backstepping, and other model-based approaches [10, 11]. PI controllers remain the most widely used due to their ease of implementation and linear design, as seen in works such as [12, 13], where DC-link voltage stability was achieved under steady-state conditions but showed degraded performance under fast transients and disturbances. To overcome the sensitivity and limited robustness of PI controllers, SMC has been proposed in various studies for its strong robustness against system uncertainties and external perturbations; however, it often introduces chattering phenomena that can stress power electronic components [14, 15]. Backstepping control, as demonstrated in [16], offers a systematic nonlinear control design approach that improves system stability and dynamic response; however, it requires precise system modeling and may be computationally intensive for real-time applications. Other researchers have explored predictive and Lyapunov-based controllers to enhance tracking performance and robustness, though they often involve complex mathematical formulations [17]. Despite the progress, these traditional regulators generally lack adaptability, especially under rapidly changing environmental conditions typical in renewable energy systems, thus motivating the need for intelligent and data-driven control strategies [18]. In response to the limitations of conventional controllers, recent research has increasingly focused on intelligent control techniques for DC-link voltage regulation in power electronic converters, especially in renewable energy systems [19, 20]. Fuzzy logic controllers (FLCs), widely reported in the literature [21], have shown superior adaptability and robustness in handling system nonlinearities without requiring an exact mathematical model [22]. However, their performance heavily depends on the design of membership functions and rule bases, which often rely on expert knowledge. Artificial neural networks (ANNs) have also been employed to approximate complex nonlinear functions and adapt to dynamic conditions, offering high precision and learning capability. Nonetheless, ANNs require extensive training data and may suffer from overfitting or slow convergence [23]. Hybrid approaches, such as adaptive neuro-fuzzy inference systems, aim to combine the strengths of fuzzy logic and neural networks, providing enhanced accuracy and adaptive learning, though at the cost of increased computational complexity [24]. Other optimisation-based techniques, including genetic algorithms and particle swarm optimisation, have been utilised to auto-tune controller parameters for optimal performance under varying operating conditions [25]. More recently, reinforcement learning (RL) has gained attention for its ability to learn optimal control policies through interaction with the environment, although its deployment in real-time systems remains challenging due to stability concerns and exploitation trade-offs [26]. While these smart controllers offer significant improvements over classical methods, they often require careful tuning, validation, and computational resources, motivating the development of interpretable and efficient machine learning models such as the M5-Pruned (M5P) decision tree proposed in this work.

This study introduces an innovative control methodology utilising the M5P algorithm for DC-link voltage regulation within a direct power control-grid voltage modulation (DPC-GVM) context, addressing the limitation of classical and conventional intelligent controllers. The M5P algorithm stands out by combining the transparency and simplicity of decision trees with the predictive accuracy of linear regression models [4]. It generates a tree structure where each leaf node has a linear model instead of a constant value, allowing it to capture both discrete decision rules and continuous relationships with high accuracy [27]. The motivation behind adopting M5P lies in its ability to model complex, nonlinear behaviours inherent in power electronic systems without the need for extensive tuning or training data [4, 27].

The key novelties and innovations of the proposed M5P DC-link voltage controller lie in its ability to learn system behaviour through a data-driven approach and avoid the need for manual tuning of control gains. It provides improved decoupling between the active and the reactive power, leading to improved control accuracy. Additionally, the controller significantly decreases total harmonic distortion (THD), contributing to higher power quality [28]. Its robust dynamic performance under varying operating conditions ensures consistent system behaviour even in the face of external disturbances. By integrating the M5P algorithm into the DPC-GVM scheme, the proposed controller overcomes the typical interdependence between the DC-link voltage and the active power, offering faster transient response and improved system stability. The proposed M5P-based control strategy introduces a powerful, interpretable, and adaptive solution for intelligent DC-link voltage regulation in PV systems. Its design bridges the gap between traditional rule-based systems and black-box machine learning models, providing a practical and effective alternative for next-generation power electronics control. This work contributes to the ongoing advancement of intelligent control in renewable energy applications and opens pathways for further integration of explainable AI techniques in real-time energy management systems. The overall configuration of the proposed DPC-GVM system, including the PV generator, boost converter, voltage source inverter (VSI), filter, and grid interface, is illustrated in Figure 1. This global representation highlights the integration of the DC-link voltage regulation loop with the intelligent controller.

2 | Topological Modelling (System Modelling)

The proposed structure is formed of a PV generation linked to the DC-link via a DC/DC boost converter operating under a maximum power point tracking (MPPT) algorithm; the regulated DC-link voltage feeds a three-phase VSI, which delivers power to the grid through an LC filter that suppresses high-frequency harmonics and ensures compliance with grid standards. For DC-link voltage regulation, three control techniques are integrated: a PI controller as a conventional linear benchmark, an FLC for enhanced robustness under nonlinear conditions, and the proposed M5P decision tree algorithm, a data-driven and self-adaptive approach capable of capturing nonlinearities and parameter variations with high precision. Within this framework, the GVM-DPC scheme directly modulates inverter voltages, yielding improved dynamic performance.

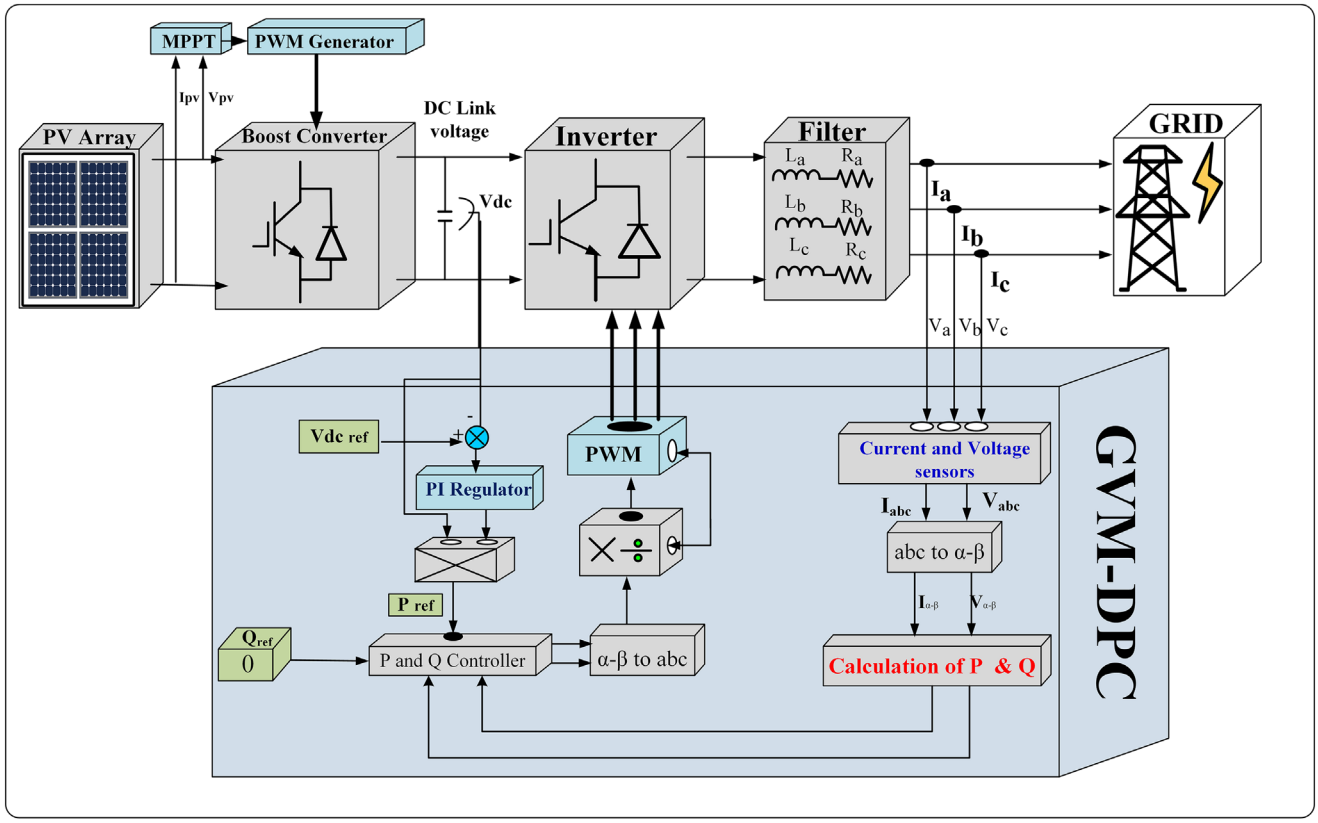

FIGURE 1 | Global representation of the DPC-GVM technique.

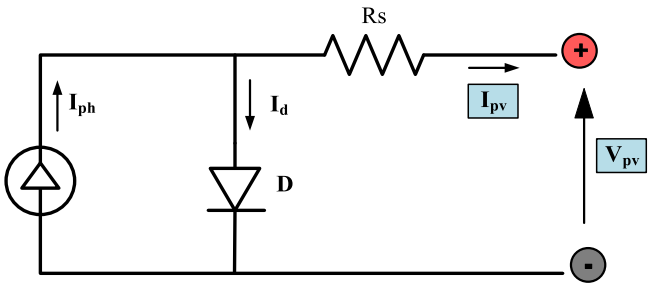

FIGURE 2 | PV cell simplified circuit.

2.1 | Photovoltaic Generator

The equivalent representation of the PV cell using the single-diode model, including photocurrent, diode, and parasitic resistances, is illustrated in Figure 2. In the present work, the PV generator is represented as a current source using the single-diode equivalent circuit, which accounts for photocurrent, diode characteristics, and parasitic resistances [29], and can be expressed as

$$I_{pv} = I_{ph} - I_0 \left[\exp\left(\frac{q\left(V_{pv} + R_s \cdot I_{pv}\right)}{AN_s K T_j} \right) - 1 \right] - \frac{V_{pv} + R_s \cdot I_{pv}}{R_{sh}} \tag{1}$$

The PV array is obtained by connecting cells in series and parallel to achieve the required voltage and current ratings [29]. To guarantee that the PV system consistently operates at its optimal power, the MPPT strategy is employed. This control method is crucial in order to maximise the energy output from PV generation systems, as stated in [30–32].

2.2 | Modelling of Voltage Source Inverter

This section depicts the mathematical representation of a three-phase VSI operating within the framework of DPC enhanced by GVM [33]. As shown in Figure 3, the VSI is connected to the grid through a simple filter, consisting of an inductor coupled in series with a resistor.

$$\begin{cases} L\dfrac{di_a}{dt} = u_a - Ri_a - V_{ag} \\ L\dfrac{di_b}{dt} = u_b - Ri_b - V_{bg} \\ L\dfrac{di_c}{dt} = u_c - Ri_c - V_{cg} \end{cases} \tag{2}$$

To simplify control design, the system is converted into the α–β stationary reference frame using the Clarke transformation.

$$\begin{bmatrix} i\alpha \\ i\beta \end{bmatrix} = \frac{2}{3} \begin{bmatrix} 1 & -\frac{1}{2} & -\frac{1}{2} \\ 0 & \frac{\sqrt{3}}{2} & -\frac{\sqrt{3}}{2} \end{bmatrix} \begin{bmatrix} ia \\ ib \\ ic \end{bmatrix} \tag{3}$$

Under balanced grid conditions, in the α–β stationary reference frame, the relationship of converter output voltage indicating line

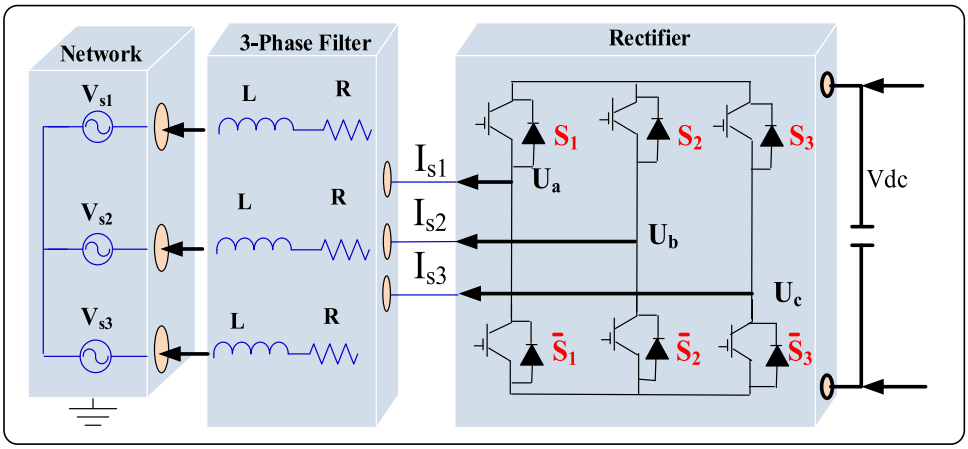

FIGURE 3 | Electric scheme of the VSI.

current and the grid voltage can be expressed as [33]

$$\begin{aligned} u_\alpha &= Ri_\alpha + L\frac{di_\alpha}{dt} + V_{\alpha,g} \\ u_\beta &= Ri_\beta + L\frac{di_\beta}{dt} + V_{\beta,g} \end{aligned} \tag{4}$$

2.3 | DPC Integrating Grid Voltage–Modulated Technique

In this context, u_α and u_β denote the output voltages of the inverter in the α–β stationary reference frame, while i_α/i_β represent the corresponding line currents. Similarly, $V_{\alpha,g}/V_{\beta,g}$ refers to grid voltages in the stationary frame [33]. The filter parameters are modelled using a resistor R and inductance L. The instantaneous active and reactive powers (P/Q) are calculated using the following expressions [33]:

$$\begin{cases} P = \frac{3}{2}\left(V_{\alpha,g}i_\alpha + V_{\beta,g}i_\beta\right) \\ Q = \frac{3}{2}\left(V_{\beta,g}i_\alpha - V_{\alpha,g}i_\beta\right) \end{cases} \tag{5}$$

P and Q denote the estimated active and reactive powers. The variation in estimated active and reactive powers is articulated by dividing (5) with terms of time as follows:

$$\begin{aligned} \frac{dP}{dt} &= \frac{3}{2}\left(i_\alpha\frac{dv_{\alpha,g}}{dt}v_{\alpha,g}\frac{di_\alpha}{dt} + i_\beta\frac{dv_{\beta,g}}{dt} + v_{\beta,g}\frac{di_\beta}{dt}\right) \\ \frac{dQ}{dt} &= \frac{3}{2}\left(i_\alpha\frac{dv_{\beta,g}}{dt}v_{\beta,g}\frac{di_\alpha}{dt} - i_\beta\frac{dv_{\alpha,g}}{dt} - v_{\alpha,g}\frac{di_\beta}{dt}\right) \end{aligned} \tag{6}$$

While the grid is undistorted, the grid voltages can be described as

$$\begin{cases} v_{\alpha,g} = V_g\ \cos(\omega t) \\ v_{\beta,g} = V_g\ \sin(\omega t) \end{cases} \tag{7}$$

where V_g represents the amplitude and $\omega = 2\pi f$ indicates the frequency of the grid voltage. By differentiating (7), the variations of the grid voltage can be expressed as follows:

$$\begin{cases} \frac{dv_{\alpha,g}}{dt} = -\omega V_g\ \sin(\omega t) = -\omega v_{\beta,g} \\ \frac{dv_{\beta,g}}{dt} = -\omega V_g\ \cos(\omega t) = \omega v_{\alpha,g} \end{cases} \tag{8}$$

Consequently, the actual active and reactive powers resulting by replacing (11) and (8) into (6) are as follows:

$$\begin{cases} \frac{dP}{dt} = -\frac{R}{L}P - \omega Q + \frac{3}{2L}\left(v_{\alpha,g}u_\alpha + v_{\beta,g}u_\beta\right) - \frac{3}{2L}V_g^2 \\ \frac{dQ}{dt} = \omega Q - \frac{R}{L}Q + \frac{3}{2L}\left(v_{\beta,g}\,u_\alpha - v_{\alpha,g}u_\beta\right) \end{cases} \tag{9}$$

The amplitude of grid voltage may then be expressed as

$$V_g = \sqrt{V_{\alpha,g}^2 + V_{\beta,g}^2} \tag{10}$$

In Equation (11), we define

$$x = [x_1\ \ x_2]^T = [P\ Q]^T \tag{11}$$

Furthermore, the controlled inputs are

$$u = [u_1\ \ u_2]^{\ T} = \left[u_\alpha\ u_\beta\right]^T \tag{12}$$

When the VSI system is modelled as a continuous-time dynamic system, its behaviour is represented in state-space form as

$$\dot{x} = f\ (x,u) = \begin{bmatrix} -\frac{R}{L}x_1 - \omega x_2\frac{3}{2L}\left(v_{\alpha,g}u_1 + v_{\beta,g}u_2 - V_g^2\right) \\ \omega x_1 - \frac{R}{L}x_2 + \frac{3}{2L}\left(v_{\beta,g}u_1 - v_{\alpha,g}u_2\right) \end{bmatrix} \tag{13}$$

$$y = h\ (x) = [x_1\ \ x_2]^T \tag{14}$$

The GVM control approach theoretically simplifies the DPC model by employing estimates to delineate the system's inputs and outputs, particularly since the actual active and reactive powers (P/Q) in the conventional DPC approach are inherently related to the system [6]. The GVM input variables may be

expressed as

$$u_P = \upsilon_{\alpha,g}\ u_1 + u_{\beta,g}u_2$$
$$u_Q = -\upsilon_{\beta,g}\ u_1 + u_{\alpha,g}u_2 \tag{15}$$

According to Equation (7), the inputs of GVM are presented in the d–q reference frame as

$$\begin{bmatrix} u_P \\ u_Q \end{bmatrix} = V_g \begin{bmatrix} \cos(\omega t) & \sin(\omega t) \\ -\sin(\omega t) & \cos(\omega t) \end{bmatrix} \begin{bmatrix} u_1 \\ u_2 \end{bmatrix} = V_g \begin{bmatrix} u_d \\ u_q \end{bmatrix} \tag{16}$$

let u_d and u_q denote the inverter voltage

$$\dot{x} = f\ \left(x, u_P.u_Q\right) = \begin{bmatrix} -\frac{R}{L}x_1 - \omega x_2 + \frac{3}{2L}\left(u_p - V_g^2\right) \\ \omega x_1 - \frac{R}{L}x_2 - \frac{3}{2L}u_Q \end{bmatrix} \tag{17}$$

The gaps between the actual values of P and Q and reference can be articulated as

$$e_P = y_{p,\,\mathrm{ref}}\ - y_p$$
$$e_Q = y_{Q,\,\mathrm{ref}}\ - y_Q \tag{18}$$

where $y_{p,\,\mathrm{ref}}$ and $y_{Q,\,\mathrm{ref}}$ denote the reference value of active and reactive powers.

Equation (15) defines v_P and v_Q as the outputs of the controller.

$$u_P = \upsilon_p + \frac{2R}{3}x_1 + \frac{2L}{3}\omega x_2 + V_g^2$$
$$u_Q = -\upsilon_Q + \frac{2L}{3}\omega x_1 - \frac{2R}{3}x_2 \tag{19}$$

So, the novel control inputs V_P and V_Q can be written as

$$\upsilon_P = \dot{y}_{1,ref} + K_{p,P}e_P + K_{p.i}\int_0^\infty e_P\ (t)\,dt$$
$$\upsilon_Q = \dot{y}_{2,ref} + K_{Q,P}e_Q + K_{Q.i}\int_0^\infty e_Q\ (t)\,dt \tag{20}$$

$Kp_{,P}$ and K_i,Q denote the positive gains of the PI controller [33, 34]. Afterwards, the errors reduce to zero, and every outcome is set up in accordance with its corresponding input. Further to differentiation, the output should persist unless no less than one of the control inputs is evident.

$$\begin{bmatrix} \dot{y}_1 \\ y_2 \end{bmatrix} = \begin{bmatrix} -\frac{R}{L}x_1 - \omega x_2 + \frac{3}{2L}\left(u_p - V_g^2\right) \\ \omega x_1 - \frac{R}{L}x_2 - -\frac{3}{2L}u_Q \end{bmatrix} \tag{21}$$

Assuming that U_p and U_Q are defined as control input as shown in Equation (19), the outputs are

$$\dot{y}_1 = \upsilon_P\ ,\ \ \dot{y}_2 = \upsilon_Q \tag{22}$$

Hence, by implementing the control rules specified in Equation (20) to the system dynamics described in Equation (25), the resulting model can be formulated as a multiple-input, multiple-output system [33]. This feedback linearisation approach effectively decouples the tracking dynamics of the active and reactive power components, leading to the following expressions:

$$\ddot{e}_P + K_{P,p}\dot{e}_P + K_{P,i}e_P\ (t) = 0$$
$$\ddot{e}_Q + K_{Q,P}\dot{e}_Q + K_{Q.i}e_Q\ (t) = 0 \tag{23}$$

Overall, by inverting (19), the control inputs are determined as

$$u_\alpha = \frac{\upsilon_{\alpha,g}u_P - \upsilon_{\beta,g}u_Q}{V_g^2}$$
$$u_\beta = \frac{\upsilon_{\beta,g}u_P + \upsilon_{\alpha,g}u_Q}{V_g^2} \tag{24}$$

2.4 | Conventional DC-Link PI-Based Voltage Control

The primary function of the DC-link voltage is to maintain a constant reference value [35]. Overlooking the losses, the power flow can be expressed as

$$P_i = P_l + C \cdot \nu_{\mathrm{dc}} \cdot V_{\mathrm{dc}} \tag{25}$$

V_{dc} serves as a new control input. $(C \cdot \nu_{\mathrm{dc}} \cdot V_{\mathrm{dc}})$ represents the power stored in the DC-link capacitor (P_C). The dynamics of the DC-link can be reformulated as a simplified, invariant, linear time-invariant system.

$$\frac{dV_{\mathrm{dc}}}{dt} = \nu_{\mathrm{dc}} \tag{26}$$

v_{dc} is the derivative of V_{dc}.

Equation (27) presents a range of control mechanisms to regulate a constant voltage. A PI controller is employed to ensure that V_{dc} remains at its reference value.

$$\nu_{\mathrm{dc}} = K_{p,\mathrm{dc}}\ \left(V_{\mathrm{dc}}^* - V_{\mathrm{dc}}\right) + K_{i,\mathrm{dc}}\ \int\ \left(V_{\mathrm{dc}}^* - V_{\mathrm{dc}}\right)\ dt \tag{27}$$

where V_{dc}* represents the DC-link reference, $K_{p,\mathrm{dc}}$ and $K_{i,\mathrm{dc}}$ signify the gain of the PI. DC-link voltage was chosen at 200 V in order to satisfy the requirement of the system design and to provide a suitable margin for reliable grid synchronisation. Additionally, the inverter topology influences this choice; a two-level inverter used in this study performs optimally with this chosen value, allowing lower modulation indices, reduced harmonic distortion, and improved power quality. Furthermore, component limitations, such as the voltage ratings of IGBTs, capacitors, and inductors, must be respected to avoid damage or failure.

$$V_{\mathrm{peak}} = \left(V_{\mathrm{RMS}}\sqrt{2}\right) \tag{28}$$

2.5 | Fuzzy Logic Control of DC-Link Voltage (Modelling and Structure)

The FLC developed in this work is built to regulate the DC bus voltage within the GVM-DPC framework. Structurally, the FLC comprises three primary stages: fuzzification, inference, and defuzzification. The controller is implemented using the Mamdani inference model, which is often used in control applications for its intuitive rule-based structure and compatibility with

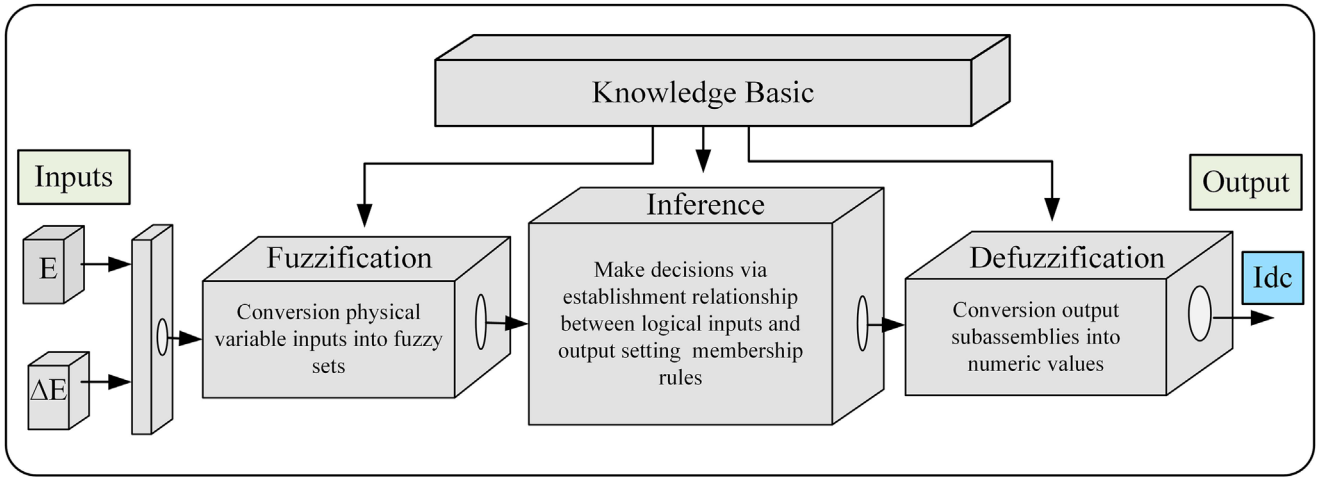

FIGURE 4 | Formation stages of fuzzy logic control.

expert knowledge representation [22]. The controller processes two input variables: the DC bus voltage error E of V_{dc} and the derivative of error ΔE of V_{dc}. These inputs are defined as

$$e_{V_{dc}}(t) = V_{dc}^{*} - V_{dc}(t) \tag{29}$$

$$\Delta e_{V_{dc}}(t) = e_{V_{dc}}(t) - e_{V_{dc}}(t - \Delta t) \tag{30}$$

$V_{dc}(t)$ is the measured voltage at time t, while the reference DC bus voltage is $V_{dc}{}^{*}$.

The fuzzification stage converts the crisp input values into fuzzy sets via appropriately defined membership functions. Throughout this study, seven linguistic terms are assigned to each input variable, resulting in a 7×7 rule base. These rules, formulated based on system behaviour and control objectives, map the fuzzy input space to the corresponding fuzzy output space [36]. The inference stage applies the fuzzy rule base to determine the control action, while the defuzzification stage converts the resulting fuzzy output into a crisp signal. The output of the controller is the reference direct current $I_{dc}{}^{*}$, which serves as the control signal to adjust the system and maintain the DC bus voltage at its desired value. This modelling approach enables the FLC to handle nonlinearities and parameter variations in the system, ensuring stable voltage regulation under both steady-state and transient conditions [37, 38]. The formation stages of the FLC, including fuzzification, inference, and defuzzification, are shown in Figure 4.

In the FLC design, different types of membership functions are utilised to enhance both transient and steady-state performance [39]. For example, trapezoidal membership functions are applied during transient conditions due to their ability to provide a stable and rapid response, enabling the control system to quickly achieve the reference levels. In contrast, triangular membership functions are employed under steady-state conditions, as they respond more sensitively to instantaneous variations in the error and its derivative [37]. This approach helps to minimise error effectively, as illustrated in Figure 4. To construct the fuzzy rule base, seven linguistic variables are defined for each of the controller's inputs and output, the error (E), the derivative of error (ΔE), and the reference current $I_{dc}{}^{*}$. These terms are NB (negative big), NM (negative medium), NS (negative small), ZE (zero), PS (positive small), PM (positive medium), and PB (positive big). The sign and magnitude of the error play a critical role in selecting the appropriate fuzzy rule. Thus, if the error, $E = M_{ref} - M_{mes}$, is significantly large and positive, the control action must also be strongly positive (PB) to raise the measured value M_{mes} accordingly. A similar rule applies in the opposite direction for negative errors. This principle is also extended to the derivative of the error ΔE to ensure a responsive and accurate control output. The defined membership functions for error, derivative of error, and the corresponding inference table are depicted in Figure 5.

3 | Proposed Machine Learning Approach (M5P Decision Tree)

Unlike deep neural networks or RL approaches, which typically require large datasets, extensive hyperparameter tuning, and high computational resources, the M5P algorithm provides a lightweight structure based on simple conditional rules and localised linear models [40]. This design enables deterministic and fast execution, making it well suited for DSP or microcontroller-based inverter hardware, where control loops operate in the microsecond range. Moreover, M5P performs reliably with moderate-sized datasets obtained from simulation, and its pruning mechanism effectively reduces overfitting, yielding a compact model with stable generalisation capabilities. Its transparent, rule-based nature further enhances interpretability, facilitating verification and validation in safety-critical grid-connected applications – an advantage not offered by Blackbox deep learning methods. Additionally, the hierarchical structure of M5P aligns naturally with the FLC-derived dataset used in this study, allowing seamless integration into the DPC-GVM framework. For these reasons, the M5P model is selected in this work for real-time DC-link voltage regulation in PV inverter systems and compared with the FLC.

3.1 | Decision Tree and M5P Algorithm

The M5P model is well suited for high-dimensional tasks and supports continuous as well as qualitative operations, even in

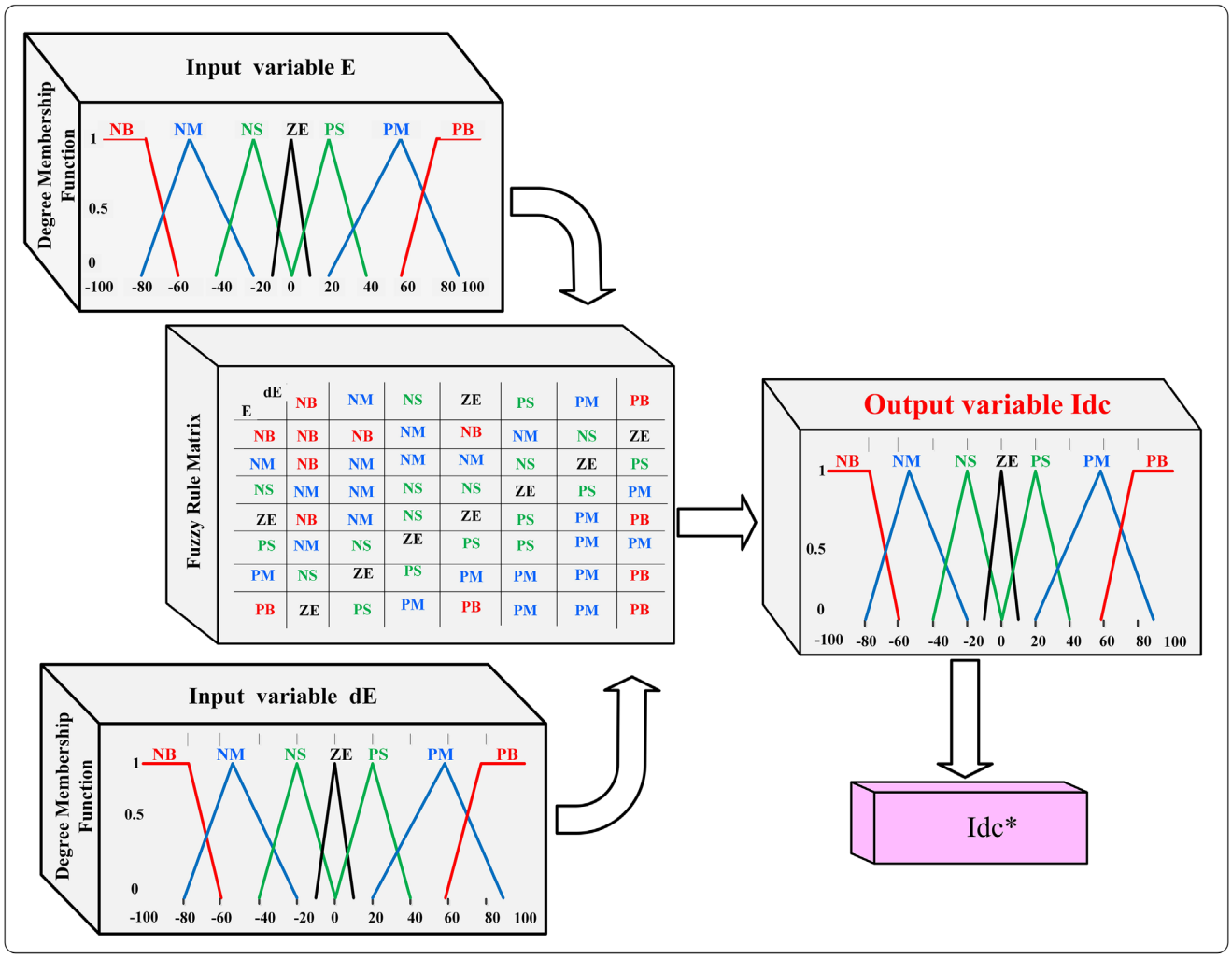

FIGURE 5 | Membership functions and inference table of fuzzy logic control.

the presence of missing or normalised values [41]. It can be applied to classification, clustering, or association rule extraction for both individuals and objects. The algorithm follows an if/then conditional structure, executed along each path from the root node to a leaf, as illustrated in Figure 6. The decision tree approach organises data into a hierarchical structure composed of roots, branches, and leaves [4]. This structure enables recursive partitioning of the data to achieve the most optimal classification or prediction outcome [33]. The process begins by selecting the most informative attribute as the root node, followed by generating branches based on the possible values of that attribute. This procedure is recursively applied to each branch using only the relevant attributes that connect the branch, progressively dividing the data space. To ensure effective classification, the purity of each resulting leaf is evaluated using a specific criterion typically based on homogeneity. The attribute that has the highest correlation with the target class is selected as the best candidate for further splitting. Decision tree development generally occurs in two phases. One involves constructing the full tree structure, wherein the dataset is partitioned into increasingly pure subsets [33]. The second one is the pruning phase, which simplifies the tree by removing branches that do not remarkably contribute to accuracy for prediction. Pruning helps reduce overfitting and improves generalisation. Once pruning is complete, the final leaves are labelled according to the distribution of observations in their respective subsets. The M5P algorithm extends the decision tree methodology to handle high-dimensional tasks and is particularly well suited for continuous, qualitative, and partially incomplete datasets. It is applicable in various domains such as classification, clustering, and association rule mining. In this study, the M5P model is leveraged to enhance control performance, and its integration is shown to be a suitable and effective alternative to the traditional PI and FLC.

To reduce prediction error, the M5P recursively splits the dataset at every node based on the most informative attribute [27], [41]. For a given node i, prediction error can be evaluated using the concept of standard deviation, denoted as (S_i), defined as

$$\mathrm{SDR} = S_i - \sum_{k=1} C \frac{N_k}{N_i} S_k \ldots \tag{31}$$

Each node (k) contains N_k training examples and a division of node i in C branches. The goal is to minimise the prediction error within each resulting subset. To quantify this, the mean absolute error (MAE) is used as a performance metric. It measures the average magnitude of the errors between the desired and actual

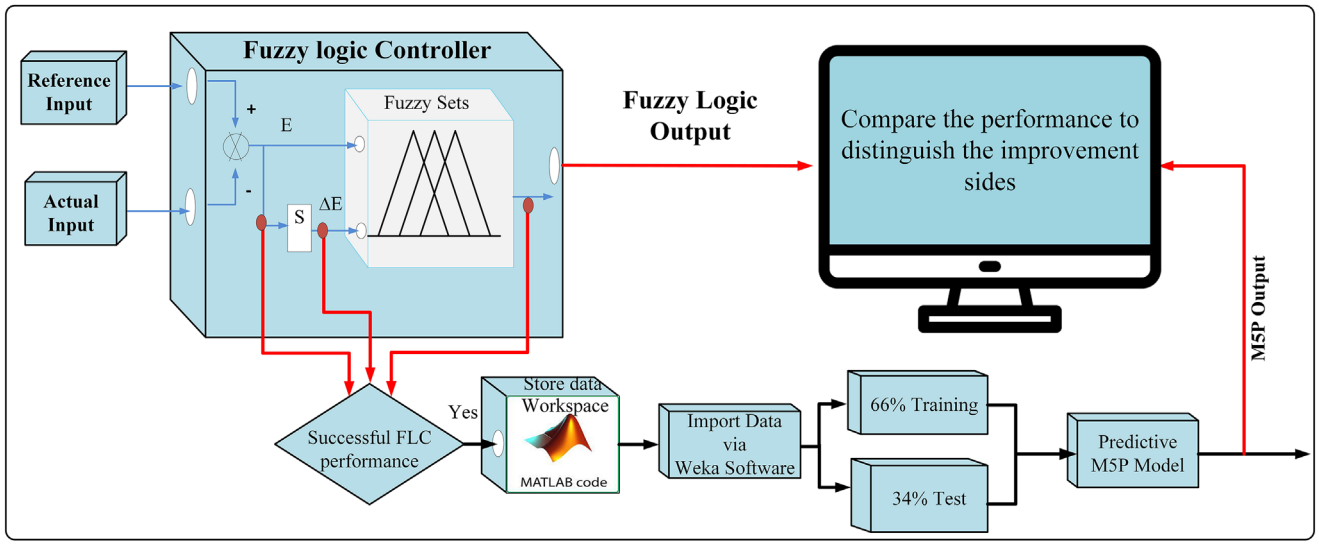

FIGURE 6 | Dataset extraction and training processes.

values [27, 41], and is calculated as follows:

$$\mathrm{MAE} = \frac{1}{n}\sum_{i=1}^{n}\left|Y_i - \hat{Y}_i\right| \tag{32}$$

Y, $\hat{Y}$, and n represent the actual value, the predicted value, and the number of data points, respectively.

$$\mathrm{RMSE} = \sqrt{\frac{\sum_{i=1}^{n}\left(\hat{Y}_i - Y_i\right)^2}{n}} \tag{33}$$

Equation (33) defines root-mean-squared error (RMSE). The coefficient factor (R) measures the training quality, expressed as

$$R = \sqrt{\frac{\sum_{i=1}^{n}\left(\hat{Y}_i - Y_i\right)^2}{\sum_{i=1}^{n}\left(\hat{Y}_i - Y_i\right)^2}} \tag{34}$$

3.2 | M5P Methodology and Structure

The M5P decision tree strategy integrates a series of optimisation strategies and structural components to enhance predictive accuracy, computational efficiency, and generalisation performance. First, model regularisation is employed to mitigate discontinuities that occur when transitioning between leaves. This is achieved by constructing a linear model at each node and using averaged weights as predicted values, ensuring smoother transitions between regions [27]. To further enhance efficiency, relevance-based splitting is used to select only the most informative features for node division, thereby minimising the number of computational operations. Within the leaf nodes, regularised linear regression models are applied to prevent overfitting and reduce the computational cost of model fitting. Model simplification is achieved by limiting the tree depth, which decreases the number of nodes and associated linear models. In addition, pruning is implemented to remove redundant or overfitted branches. This may involve pre-pruning, where growth is halted early based on criteria such as maximum depth or node purity, or post-pruning, where a fully grown tree is simplified by merging similar leaves, thereby reducing the number of regressions and computational burden [27, 41, 42].

From a structural perspective, M5P offers several key features:

a. Attribute transformation: Continuous or natural attributes can be transformed into binary or categorical forms via embedded linear models to optimise decision-making.

b. Missing values management: M5P demonstrates flexibility in managing incomplete datasets through imputation (e.g., replacing missing values with the mean or median) or by ignoring the attribute during analysis. While the latter may slightly reduce accuracy, it maintains operational continuity.

c. Pruning: It is used to simplify the decision tree and enhance generalisation. Pre-pruning limits tree growth based on depth or node purity, while post-pruning removes overfitted branches after full growth. In M5P, pruning eliminates redundant or noisy branches, reducing complexity without compromising accuracy.

d. Linear regression at terminal nodes: Each leaf contains a simplified linear regression model, ensuring accurate, fast predictions and making the method suitable for real-time control applications. A linear regression model can be represented mathematically as follows:

$$LM_j = \omega_{j0} + \omega_{j1}a_1 + \cdots + \omega_{jk}a_k \tag{35}$$

e. Interpretability: A major strength of M5P lies in its transparent decision-making process. Each node represents a conditional rule, and each leaf hosts an interpretable linear model, allowing clear insight into how input features influence control outputs and overall system behaviour.

Through this combination of regularisation, relevance-based splitting, pruning, and interpretability, M5P delivers a robust and computationally efficient framework suitable for both offline analysis and real-time control applications [27, 41, 42]. One of the most notable strengths of M5P also lies in its robust data

management capabilities. It effectively handles missing values, mitigates the influence of outliers, and supports normalisation or standardisation of input features. Moreover, advanced techniques such as cross-validation and data augmentation are applied to enhance the quality and diversity of the training data [27, 41, 42]. These procedures significantly increase accuracy, generalisation, and robustness [27]. In the context of this study, input and output training data are obtained via system simulations to form a specialised dataset M5P-DATA used for training the decision tree models. The goal is to enhance the conventional DPC scheme by changing the DC bus voltage controller with intelligent, M5P-based models. The overall design workflow, including the M5P-DATA extraction and control model generation process, is illustrated in Figures 6 and 7.

3.3 | Dataset Extraction Process

The dataset used in this work is derived from the inputs and outputs of the FLC for DC bus voltage regulation. This approach is motivated by the similarity in the decision-making structure of both techniques, which rely on rule-based logic (if/then format). This commonality facilitates the generation of a coherent dataset suitable for training the M5P decision tree [27]. Prior to data collection, the fuzzy controller is carefully designed and implemented, as illustrated in Figures 4 and 5, respectively. This controller is then used in simulations to produce control responses under various operating conditions. The collected dataset encapsulates control decisions and system states, which are later used to train the M5P model. To optimise the learning process, the pruning mechanism within the M5P algorithm is applied. This helps reduce model complexity by eliminating redundant branches, thereby simplifying the decision-making structure without compromising accuracy [42].

3.4 | Model Implementation in WEKA

The implementation and training of the M5P controller are performed using WEKA (version 3.8.6), an open-source platform widely recognised for machine learning and data mining. WEKA offers a comprehensive suite of tools for data preprocessing, classification, clustering, regression, and association rule mining [43, 44]. One of its key advantages is the ability to generate interpretable decision tree models consisting of roots, nodes, branches, and leaves, as illustrated in Figure 8. This capability makes WEKA particularly suitable for developing intelligent controllers that require both predictive accuracy and model transparency. Among WEKA's algorithms, M5P is selected for its ability to generalise from the training dataset and accurately predict outcomes for unseen operating conditions. By embedding linear regression models within the decision tree framework, M5P captures both the nonlinear decision boundaries and local linear dynamics of the control problem [44].

Table 1 illustrates the statistical performance metrics of the trained models, offering quantitative insight into their predictive accuracy and generalisation capability. Figures 6 and 7 display the M5P model's training results based on FLC-derived data, highlighting the effectiveness of the approach in modelling the nonlinear dynamics of the DPC-GVM system. The statistical and structural configuration of the trained M5P model, generated through WEKA software, is summarised in Table 2 [41–43].

TABLE 1 | Statistical training value of M5P.

Parameters	Proposed M5P model
Test mode	Split 66% train
Number of attributes	3
Number of rules	12 Rules
Time taken to build the model	0.17 s
Time taken to test model during test split	0.02 s
Correlation coefficient	0.998
MAE	0.127
RMSE	0.1456
Relative absolute error	7.8019%
Root relative squared error	6.2773
Total number of instances	20400

3.5 | Training Process Under the WEKA Software

The splitting and linear regression mechanism of the M5P decision tree, where nodes are recursively divided and terminal leaves are modelled using linear regression, is illustrated in Figure 8. Figure 9 illustrates the visualisation of the M5P decision tree model outputs for different input feature combinations, generated using WEKA software, illustrating the clustering patterns and predictive behaviour of the trained model. Each subplot (A–D) presents a scatter plot of predicted values versus selected input feature combinations, where the points are coloured according to the output classification range. The extracted dataset and clustering results generated by the WEKA software are shown in Figure 10, illustrating the distribution of predicted outputs for different input feature combinations.

4 | Simulation Results and Discussion

The evaluation of the performance of a suggested system and algorithm necessitates the implementation of comparative simulation results. To validate the conceptual insights and understand the behaviour of the proposed GVM-M5P algorithm, a series of comparative simulations were conducted to compare its performance against that of GVM-PI and GVM-FLC controllers. The findings from the simulation clearly show the efficacy of the proposed GVL-M5P control method, revealing multiple performance advantages. The approach delivers high accuracy in grid current regulation, ensuring close tracking of reference values and adherence to performance criteria. It also enhances system stability across a large range of operating conditions, including sudden disturbances and dynamic changes. Additionally, the method significantly improves transient performance by reducing response time and enabling faster convergence to a steady state. Furthermore, it achieves a noticeable reduction of THD, resulting in smoother current waveforms and enhanced power

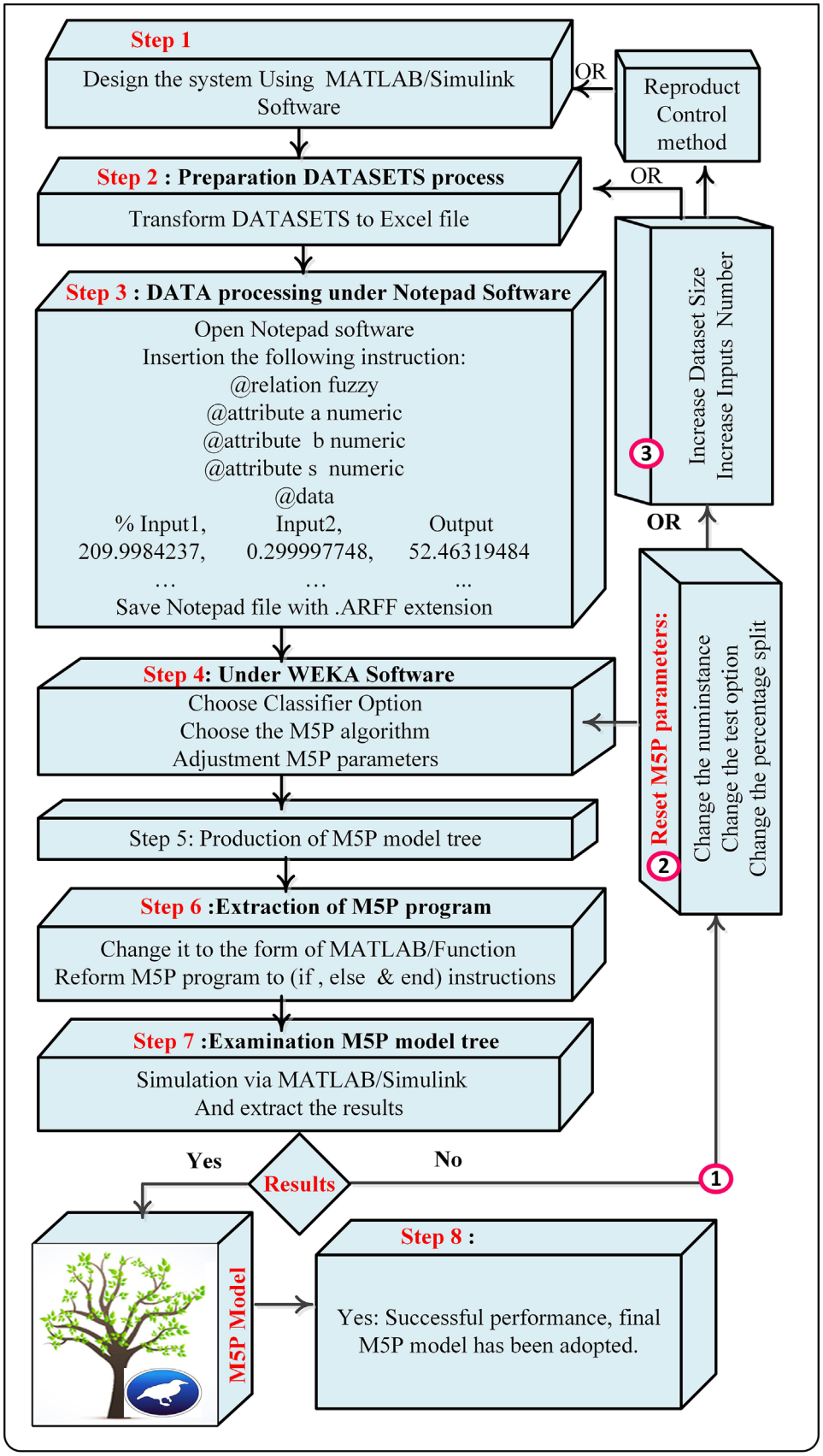

FIGURE 7 | Research methodology outline.

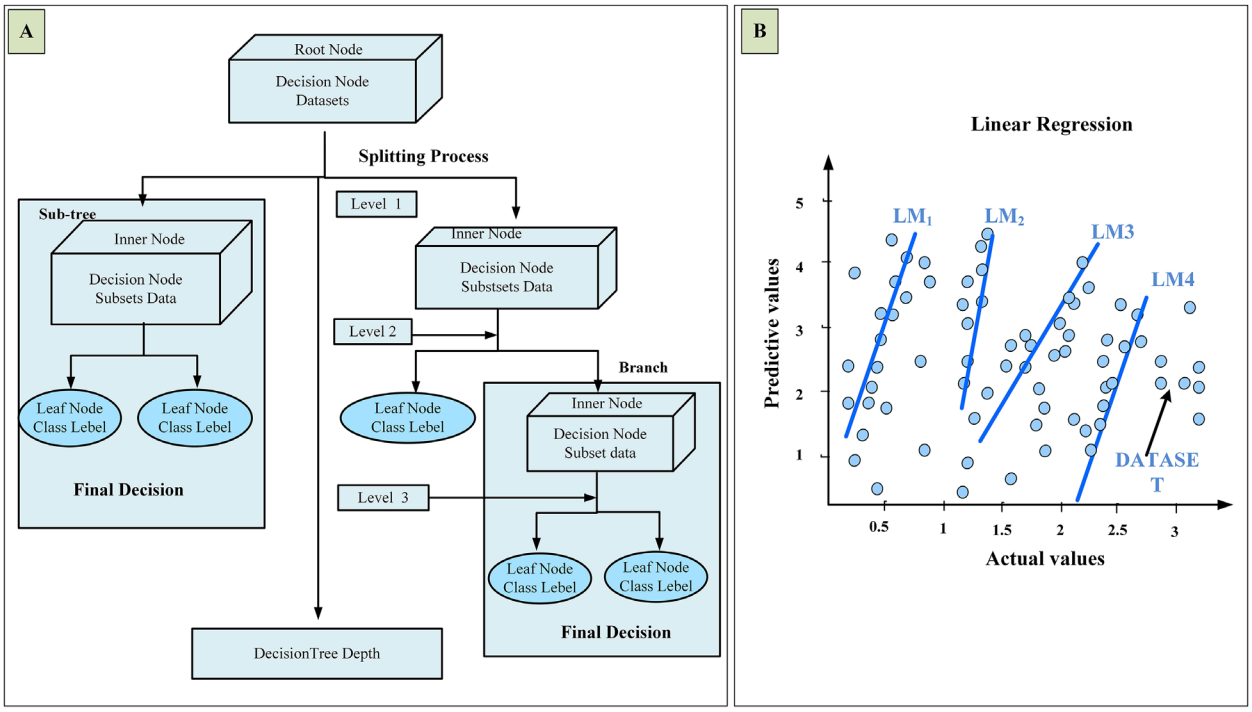

FIGURE 8 | Splitting and linear regression mechanism.

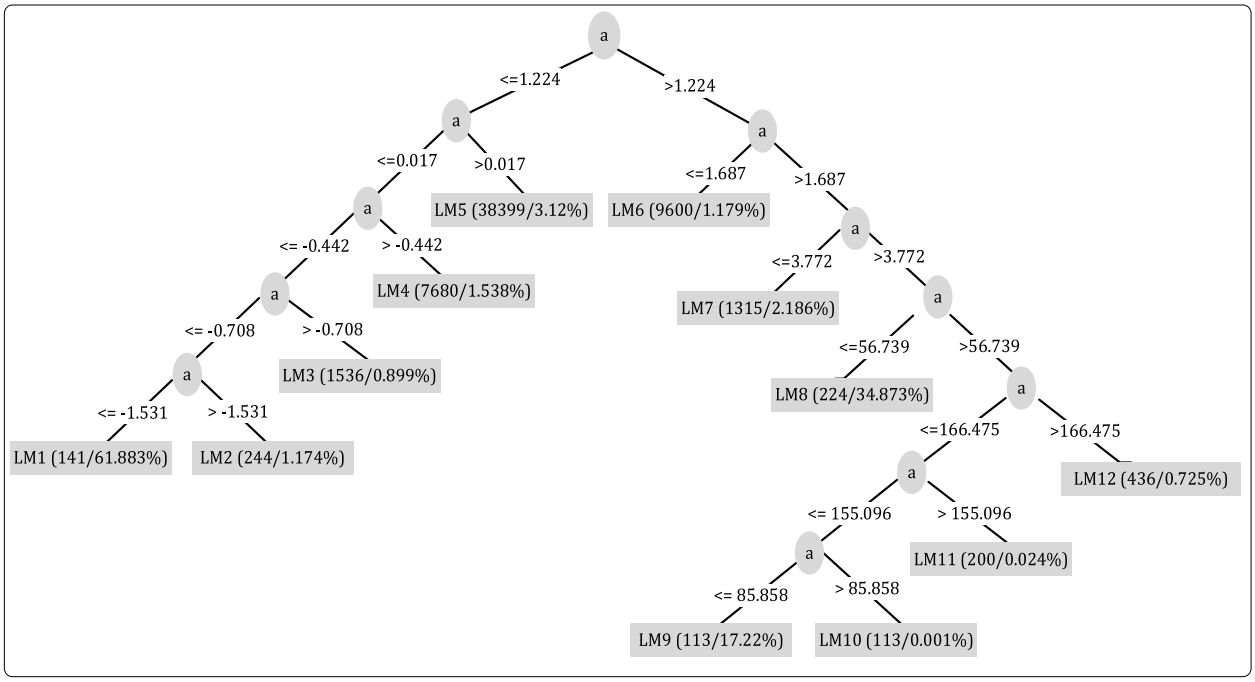

FIGURE 9 | Proposed M5P decision tree.

delivery to the grid. The detailed electrical and environmental parameters adopted for the simulated PV converter grid system are listed in Table 3 [29–33].

4.1 | Transient State Performance of System

4.2 | Reactive Power Variation Performance of System

4.3 | Steady-State Performance of System

Figure 10 illustrates the dynamic response of the DC-link voltage under a transient disturbance for the three control strategies (PI, FLC, and proposed M5P), compared against the reference value. The reference DC bus voltage is initially established at 200 V, faces a sudden increase to 250 V at $t = 0.2$ s, and then drops to 235 V at $t = 0.4$ s throughout the test; the reference reactive power is maintained at zero. The PI controller exhibits a

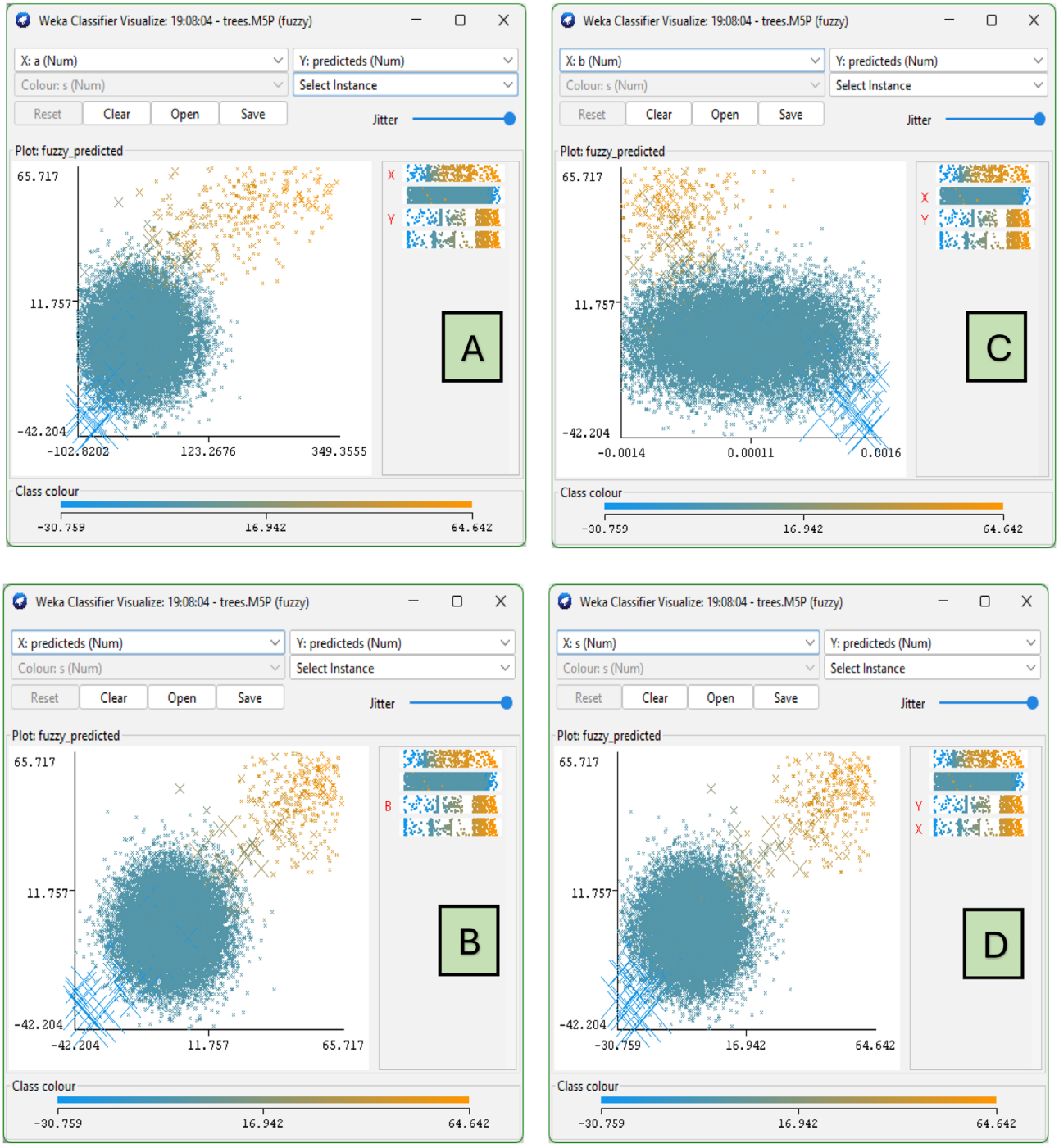

FIGURE 10 | Data extracted from the proposed method via WEKA software.

pronounced overshoot, surpassing 235 V before gradually settling, and oscillatory behaviour immediately following the transient event, while the FLC demonstrates improved damping but still deviates from the reference. In contrast, the proposed M5P controller achieves the fastest settling with minimal overshoot and closely tracks the reference voltage, highlighting its superior transient performance and voltage stability.

Figure 11 presents the active power response during transient conditions. The magnified window (highlighted yellow) reveals a detailed view of the transient peak that occurs between 0 and 0.0075 s. The PI and FLC controllers show significant deviations and slower convergence towards the reference value, with the PI controller displaying the largest peak and settling time. The proposed M5P controller, however, exhibits a rapid and smooth transition, quickly stabilising to the desired active power level with minimal overshoot and oscillation. The zoom-in box clearly shows how the proposed method suppresses transient oscillations, offering smoother and more controlled behaviour during the switching event.

Figure 12 shows the transient behaviour of reactive power to external disturbances caused by changes in DC-link voltage references under the three control approaches. The highlighted zoom-in

TABLE 2 | Information of M5 pruned model.

Run information	LM num1 = 0.2399 * a − 11.2141
Scheme: weka.classifiers.trees.M5P-M 100.0-num-decimal-places 4	LM num2 = 0.035 * a − 3.9933
Relation: fuzzy	LM num3 = 0.0068 * a − 3.7434
Instances: 60001	LM num4 = 0.0014 * a − 3.4662
Instances: 60001	LM num5 = 0.0002 * a − 2.9145
Attributes: 3	LM num6 = 0.0008 * a − 2.4618
a, b, s	LM num7 = 0.0048 * a − 2.1408
Test mode:	LM num8 = 0.4547 * a + 0.6899
split 66.0% train, remainder test	LM num9 = 0.1506 * a + 29.1636
Classifier model (full training set)	LM num10 = 0.0925 * a + 33.6086
M5 pruned model tree: (using smoothed linear models)	LM num11 = 0.0905 * a + 33.7961
a ≤ 1.22:	LM num12 = 0.0901 * a + 33.8546
| a ≤ 0.017:	
| | a ≤ −0.442:	
| | | a ≤ −0.708:	Number of rules: 12
| | | | a ≤ −1.531: LM1 (141/61.883%)	Time taken to build model: 0.17 s
| | | | a > −1.53: LM2 (244/1.174%)	
| | | a > −0.708: LM3 (1536/0.899%)	
| | a > −0.442: LM4 (7680/1.538%)	Evaluation on test split
| a > 0.017: LM5 (38399/3.12%)	Time taken to test model on test split: 0.02 s
a > 1.224:	
| a ≤ 1.687: LM6 (9600/1.179%)	
| a > 1.687:	*Summary*
| | a ≤ 3.772: LM7 (1315/2.186%)	Correlation coefficient 0.998
| | a > 3.772:	MAE 0.127
| | | a ≤ 56.739: LM8 (224/34.873%)	RMSE 0.4156
| | | a > 56.739:	Relative absolute error 7.8019%
| | | | a ≤ 166.475:	Root relative squared error 6.2773%
| | | | | a ≤ 115.096:	Total Number of Instances 20400
| | | | | | a ≤ 85.858: LM9 (113/17.22%)	
| | | | | | a > 85.858: LM10 (113/0.001%)	
| | | | | a > 115.096: LM11 (200/0.024%)	
| | | | a > 166.475: LM12 (436/0.725%)	

(Continues)

TABLE 2 | (Continued)

TABLE 3 | Parameters of system.

Parameters	Value (unit)	Parameters of PV	Value (unit)
DC-link voltage, V_{dc}	200 (V)	Open-circuit voltage, V_{oc}	57 (V)
Filter inductor, L	10 (μH)	Short Circuit Current, I_{sc}	4.6(A)
Filter inductor, R	20 (Ω)	Maximum power voltage, V_{mp}	47 (V)
DC-link capacitor, C	1100 (μF)	Maximum power current, I_{mp}	4.26 (A)
Sample time, T_s	1e−5 (s)	Working temperature, T	[−45, +85] (Co)

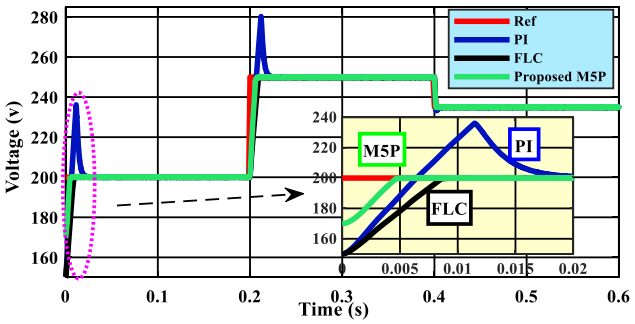

FIGURE 11 | DC-link voltage during transient state.

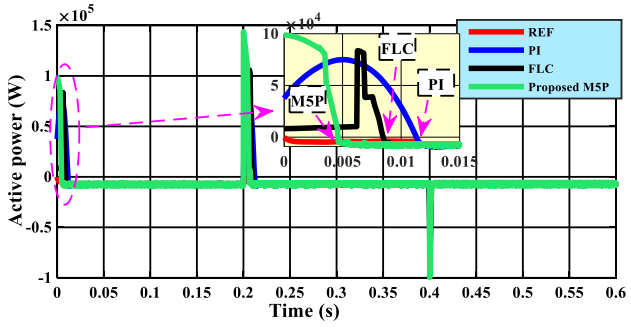

FIGURE 12 | Active power during transient state.

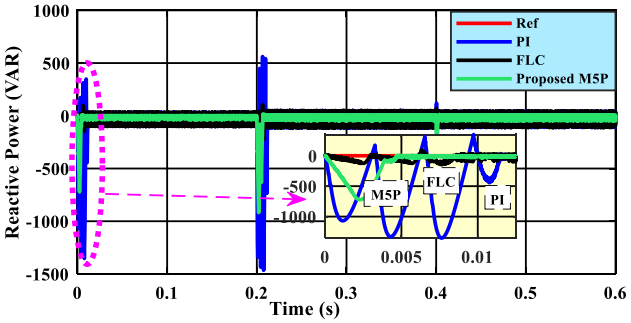

FIGURE 13 | Reactive power response during transient state.

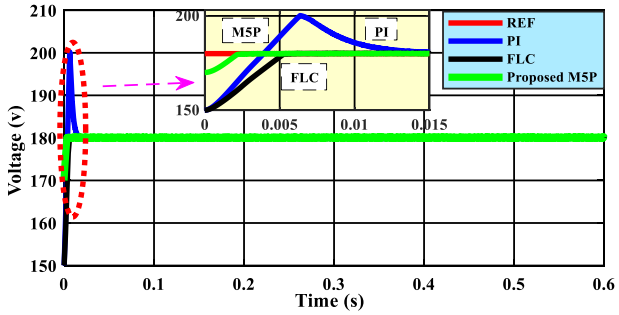

FIGURE 14 | Response of DC-link voltage under reactive power variation.

region shows that the PI controller suffers from oscillations and large amplitude deviations, reaching peaks below −1400 VAR and a prolonged settling period, while the FLC reduces these oscillations but still displays sustained oscillatory behaviour. On the other hand, the proposed M5P controller demonstrates significantly enhanced performance. It rapidly suppresses the disturbance impact and stabilises the system close to the reference value with minimal oscillations. The initial response zone (highlighted with a magenta ellipse) further confirms the superior damping capability of the proposed approach.

Figure 13 displays the DC-link voltage trajectories for PI, FLC, and proposed M5P controllers during a reactive power variation event. The PI controller experiences significant overshoot and slow settling, while the FLC shows improved damping but still deviates from the reference. The proposed M5P controller exhibits the most stable and accurate response, rapidly converging to the reference value with minimal overshoot, confirming its superior voltage regulation capability under changing reactive power conditions.

Figure 14 compares the active power response of each control strategy during the reactive power disturbance. The PI and FLC controllers display substantial deviations, overshoot, and prolonged oscillations before stabilising. In contrast, the proposed M5P controller demonstrates a swift and smooth transition to the desired active power set point, with minimal transient oscillation and steady-state error. This highlights the M5P controller's enhanced adaptability and accuracy in active power control under reactive power variation.

Figure 15 illustrates the system's reactive power response following a step change in reference. The PI controller results in

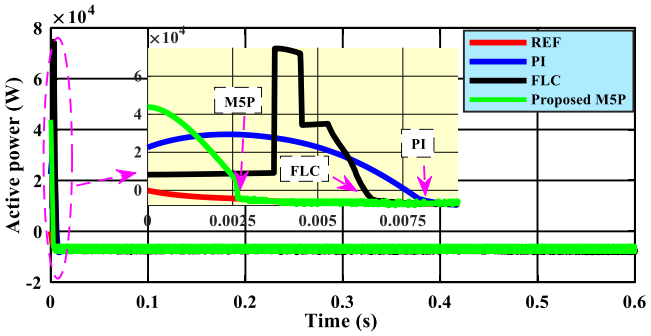

FIGURE 15 | Active power response under reactive power variation.

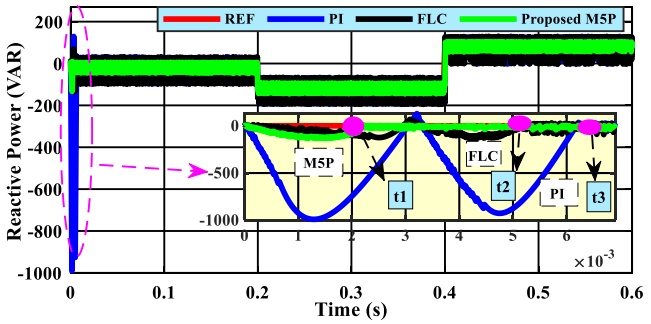

FIGURE 16 | Reactive power response under reactive power variation.

large oscillations and delayed settling, while the FLC reduces oscillatory behaviour but does not eliminate steady-state error. The proposed M5P controller achieves rapid convergence to reference, maintaining a stable and consistent reactive power profile with negligible overshoot and disturbance. The zoomed-in view further emphasises the M5P controller's superior transient and steady-state performance compared to the conventional PI and FLC strategies.

Figure 16 depicts the steady-state performance of the DC-link voltage for the PI, FLC, and proposed M5P controllers compared to the reference value. The PI and FLC controllers show noticeable fluctuations and deviations around the reference voltage, indicating less precise regulation. In contrast, the proposed M5P controller consistently maintains the DC-link voltage at the reference level, with minimal variation. This demonstrates the M5P controller's superior steady-state accuracy and voltage stability.

Figure 17 presents the steady-state active power response under all control strategies. Both PI and FLC controllers exhibit persistent oscillations and deviations from the reference active power, while the proposed M5P controller quickly settles and closely matches the reference value. The reduced oscillatory behaviour and improved tracking accuracy of the M5P method highlight its effectiveness in maintaining active power stability during steady-state operation.

Figure 18 shows the steady-state reactive power profiles for the three controllers. The PI and FLC controllers suffer from significant oscillations and frequent deviations from reference, whereas the proposed M5P controller demonstrates a stable and smooth

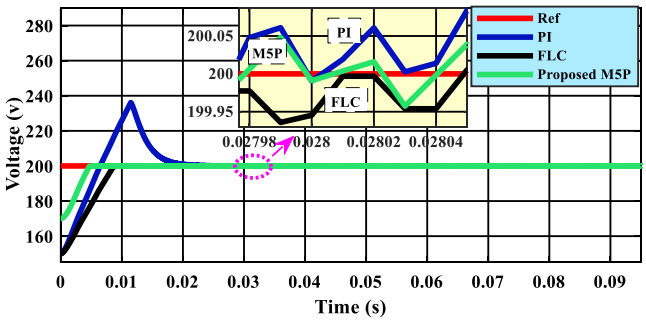

FIGURE 17 | DC-link voltage in steady state.

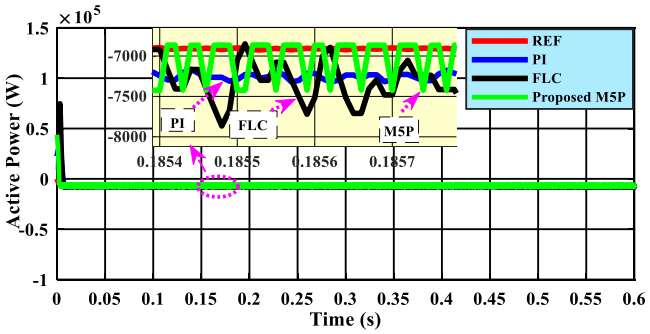

FIGURE 18 | Active power in steady state.

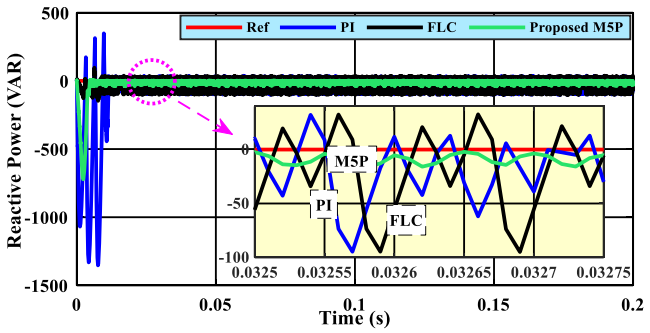

FIGURE 19 | Reactive power in steady state.

response with minimal steady-state error. The zoomed detail further confirms the M5P controller's ability to suppress oscillations and precisely regulate reactive power, ensuring optimal power quality and system reliability.

The conventional PI controller exhibits significant overshoot (±18 A), as shown in Figure 19. Current distortions persist beyond 0.15 s, indicating limited dynamic response to voltage disturbances. The PI controller demonstrates significant low-order harmonic pollution (0). Harmonics up to the 15th order exceed 0.008% of the fundamental, with pronounced 5th and 7th harmonics. The THD of 0.57% is comfortably far from the IEEE 519-2014 limit for distribution systems (<5%).

Figure 20 demonstrates that FLC reduced THD marginally to 0.53% versus PI, suppressing harmonics above order 11. However, a harmonic component of 0.05% appears from orders 5 and 7. The proposed M5P strategy introduces robust current control, as illustrated in Figure 21, reducing the THD to 0.20% – a 62%

TABLE 4 | Performance benchmarking.

Controller	THD (%)	Worst harmonic (%)
PI	0.57	0.015 (7th)
FLC	0.53	0.050 (7th)
Proposed M5P	0.20	0.027 (5th)

improvement over FLC and 65% over PI, as shown in Figure 22. Harmonic magnitudes collapse below 0.005% above the 7th order, demonstrating effective switching frequency ripple attenuation. Critically, the 3rd harmonic vanishes, confirming the strategy's robustness against grid imbalances. A quantitative comparison of harmonic performance for all controllers is presented in Table 4, confirming the superior THD suppression capability of the proposed M5P approach [4, 23, 40]. The complete harmonic spectrum comparison of the PI, FLC, and proposed M5P controllers is shown in Figure 23, which clearly demonstrates the substantial reduction of low-order harmonics and verifies the overall improvement in power quality achieved by the proposed intelligent control method.

In summary, the proposed M5P controller demonstrates superior performance over traditional PI and FLC strategies, offering improved accuracy, reduced overshoot, faster settling time, and enhanced reference tracking under dynamic conditions. Its integration with GVM results in a highly responsive and robust control strategy, ensuring effective regulation of the DC-link voltage, the active power, and the reactive power. The M5P controller demonstrates robust disturbance rejection and improved transient and steady-state stability, thereby enhancing the reliability and power quality of grid-connected systems.

5 | Conclusion

This study introduced an intelligent enhancement to the DPC strategy for three-phase PV inverters by integrating GVM and assessing three DC-link voltage control techniques: PI, fuzzy logic control, and a novel M5P decision tree–based algorithm. The results demonstrated the limitations of conventional PI controllers in terms of adaptability, precision, and dynamic performance, while FLC, although more effective in handling nonlinearities, still exhibited constraints in achieving optimal control accuracy.

The proposed M5P-based controller, embedded within the DPC-GVM framework, outperformed both PI and FLC by providing a data-driven, self-adaptive, and computationally efficient solution. It achieved a significant reduction in THD to 0.20%, enabled complete decoupling of active and reactive powers, and improved overall system stability without requiring manual gain tuning. The simulation outcomes validated the robustness and effectiveness of the method under both steady-state and transient conditions, establishing the DPC-GVM-M5P approach as a promising next-generation control solution for PV grid integration.

Future research may focus on the real-time implementation of the proposed controller and investigate its performance under

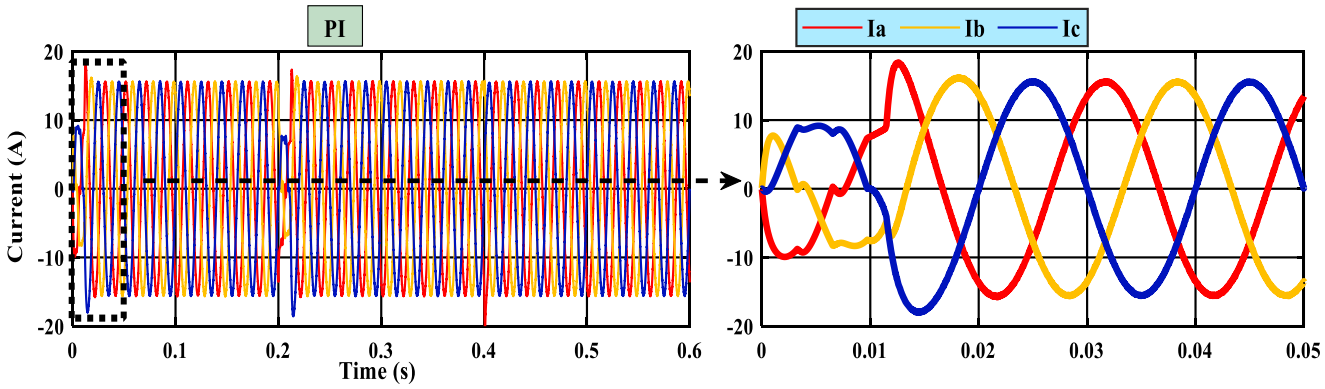

FIGURE 20 | PI controller performance of the three-phase current.

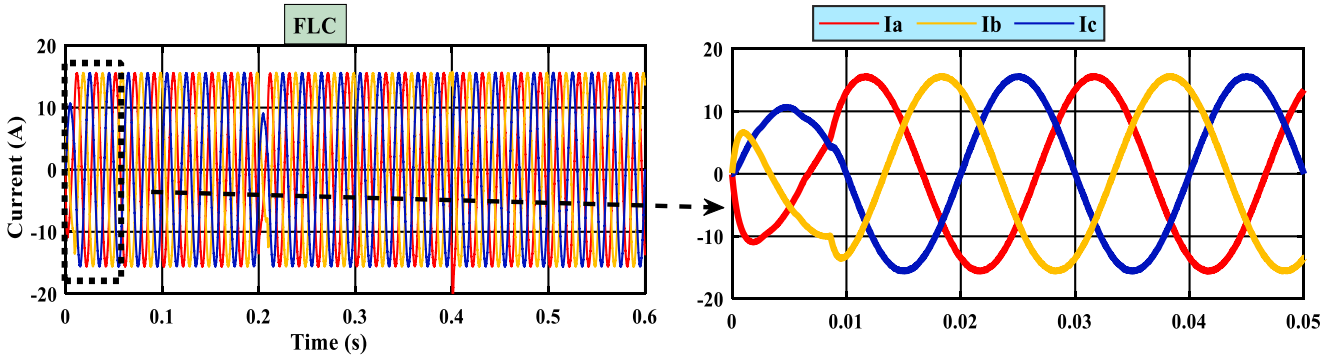

FIGURE 21 | FLC controller performance of the three-phase current.

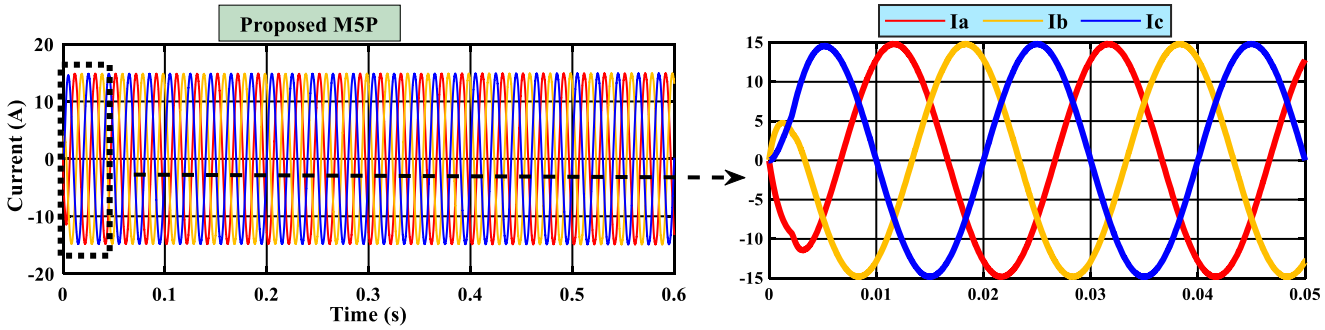

FIGURE 22 | Proposed M5P controller performance of the three-phase current.

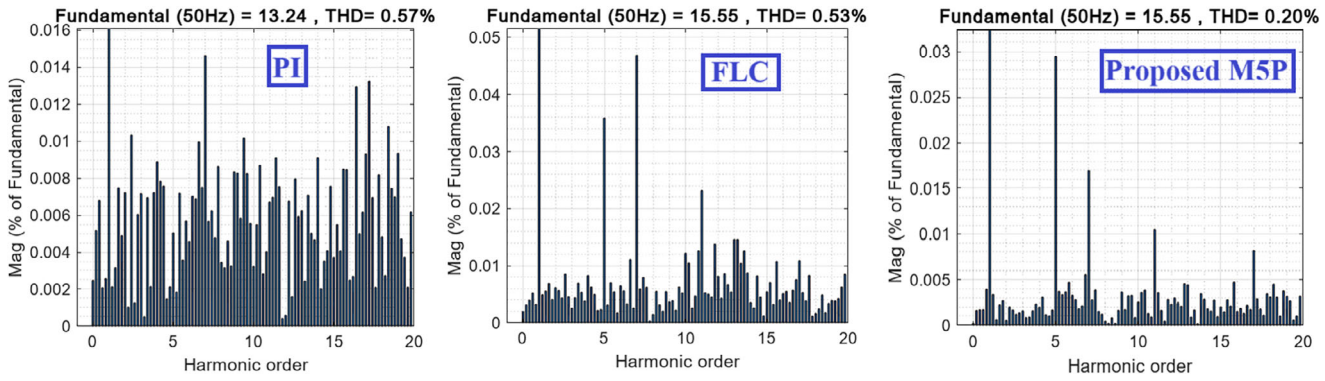

FIGURE 23 | Spectrum of THD with PI-FLC and the proposed M5P control.

fluctuating irradiance, grid disturbances, and hardware-in-the-loop environments to further validate its practical applicability.

Nomenclature

Abbreviations

GVM	grid voltage modulation
PWM	pulse width modulation
VSI	voltage source inverter
PCH	port-controlled Hamiltonian
MPPT	maximum power point tracking
DPC	predictive direct power control
ANN	artificial neural network
SMC	sliding-mode control
RMSE	root-mean-squared error

Symbols

I_0	diode saturation current
P_m	maximum power
u_α, u_β	outputs of inverter voltages in the $\alpha\beta$ frame
V_{mp}	maximum power voltage
u_1, u_2	inputs of inverter voltages
I_{mp}	maximum power current
N_{S}	number of photovoltaic cells connected in series
E_{g}	gap energy
N_{P}	number of photovoltaic cells connected in parallel
e_P, e_Q	active and reactive power errors
V_g	voltage of grid
T_{S}	sample time
R	resistance of the filter
y_P, y_Q	measured active and reactive powers
L	inductance of the filter
$y_{p,\,\mathrm{ref}}$, $y_{Q,\,\mathrm{ref}}$	reference value of active and reactive powers
C	DC-link capacitor
G	solar irradiance ($\mathrm{W/M^2}$)
I_{SC}	short-circuit current
U_{P}	GVM control inputs of active power
V_{OC}	open-circuit voltage
U_Q	GVM control inputs of reactive power
Z^{-2}, Z^{-5}	memorised previous input value of error
K_{p}	proportional gain of PI controller
u_d, u_q	GVM inputs in the d–q reference frame
K_i	integral gain of PI controller

Author Contributions

Khechafi Sofiane wrote the main manuscript, Bouchhida Ouahid and Bouraiou Abdelouahab supervised this work, Mujammal Ahmed Hasan Mujammal developed the software, Mohammed Abdulelah Albasheri validated the work, data curation, validation, supervision, resources, writing – review & editing, Mohit Bajaj and Olena Rubanenko were responsible for funding acquisition and contributed to writing – review & editing, and all authors reviewed both the final manuscript and the revised version of the manuscript.

Funding

The authors have nothing to report.

Conflicts of Interest

The authors declare no conflicts of interest.

Data Availability Statement

The data that support the findings of this study are openly available in the M5P-for-GVM-DPC repository at: https://github.com/Sofiantech007/M5P-for-GVM-DPC.

References

1. A. Q. Al-Shetwi, M. A. Hannan, H. M. K. Al-Masri, and M. Z. Sujod, "Latest Advancements in Smart Grid Technologies and Their Transformative Role in Shaping the Power Systems of Tomorrow: An Overview," *Progress in Energy* 7, no. 1 (January 2025): 012004, https://doi.org/10.1088/2516-1083/ada198.

2. M. A. Basit, S. Dilshad, R. Badar, and S. M. Sami ur Rehman, "Limitations, Challenges, and Solution Approaches in Grid-Connected Renewable Energy Systems," *International Journal of Energy Research* 44, no. 6 (2020): 4132–4162, https://doi.org/10.1002/er.5033.

3. M. Bajaj and A. K. Singh, "Grid Integrated Renewable DG Systems: A Review of Power Quality Challenges and State-of-the-Art Mitigation Techniques," *International Journal of Energy Research* 44, no. 1 (2020): 26–69, https://doi.org/10.1002/er.4847.

4. M. A. H. Mujammal, A. Moualdia, D. Boudana, P. Wira, and A. Cherifi, "Implementation of Smart Direct Power Control Strategy Based on M5-Pruned Algorithm for Three-Phase Pulse Width Modulation Rectifier," *Energy* 315 (January 2025): 134417, https://doi.org/10.1016/j.energy.2025.134417.

5. A. Moualdia, S. Boulkhrachef, and P. Wira, "Direct Torque Control-Fuzzy Type 2 for Direct Current Link Voltages Balancing of the Five-Level Cascade Converters Used in a Wind Energy Conversion System," *Advances in Systems Science and Applications* 22, no. 1 (April 2022): 15–34, 10.25728/assa.2022.22.1.882. Art. no. 1.

6. Y. Gui, C. Kim, C. C. Chung, J. M. Guerrero, Y. Guan, and J. C. Vasquez, "Improved Direct Power Control for Grid-Connected Voltage Source Converters," *IEEE Transactions on Industrial Electronics* 65, no. 10 (October 2018): 8041–8051, https://doi.org/10.1109/TIE.2018.2801835.

7. J. Hu, L. Shang, Y. He, and Z. Q. Zhu, "Direct Active and Reactive Power Regulation of Grid-Connected DC/AC Converters Using Sliding Mode Control Approach," *IEEE Transactions on Power Electronics* 26, no. 1 (January 2011): 210–222, https://doi.org/10.1109/TPEL.2010.2057518.

8. J. D. Rojas, O. Arrieta, and R. Vilanova, "Industrial PID Control," in *Industrial PID Controller Tuning: With a Multiobjective Framework Using MATLAB®*, ed. J. D. Rojas, O. Arrieta, and R. Vilanova (Springer, 2021), 5–19, https://doi.org/10.1007/978-3-030-72311-8_2.

9. J. D. Rojas, O. Arrieta, and R. Vilanova, "PID Tuning as a Multiobjective Optimization Problem," in *Industrial PID Controller Tuning: With a Multiobjective Framework Using MATLAB®*, ed. J. D. Rojas, O. Arrieta, and R. Vilanova (Springer, 2021), 91–113, https://doi.org/10.1007/978-3-030-72311-8_7.

10. M. A. Albasheri, O. Bouchhida, Y. Soufi, A. Moualdia, and M. Mujammal, "Control and Power Management of DC Microgrid Based Wind/Battery/Supercapacitor," in *2022 IEEE 2nd International Maghreb Meeting of the Conference on Sciences and Techniques of Automatic Control*

and Computer Engineering (MI-STA), May 2022, pp. 680–685, https://doi.org/10.1109/MI-STA54861.2022.9837665.

11. A. Lunardi, L. F. Normandia Lourenço, E. Munkhchuluun, L. Meegahapola, and A. J. Sguarezi Filho, "Grid-Connected Power Converters: An Overview of Control Strategies for Renewable Energy," *Energies* 15, no. 11 (January 2022), 4151, https://doi.org/10.3390/en15114151.

12. S. Chen, J. Yao, J. Pei, et al., "Transient Stability Analysis and Improved Control Strategy for DC-Link Voltage of DFIG-Based WT During LVRT," *IEEE Transactions on Energy Conversion* 37, no. 2 (January 2022): 880–891, https://doi.org/10.1109/TEC.2021.3126855.

13. X. Yuan, F. Wang, D. Boroyevich, Y. Li, and R. Burgos, "DC-Link Voltage Control of a Full Power Converter for Wind Generator Operating in Weak-Grid Systems," *IEEE Transactions on Power Electronics* 24, no. 9 (September 2009): 2178–2192, https://doi.org/10.1109/TPEL.2009.2022082.

14. M. A. H. Mujammal, A. Moualdia, G. Lorenzini, S. Boulkhrachef, P. Wira, and M. A. Albasheri, "Three-Phase PWM Rectifier Control: Enhanced Direct Power Control With Neural Networks From Theory to Superior Reality Performance," *JESA* 57, no. 6 (December 2024): 1743–1752, 10.18280/jesa.570622.

15. L. Wu, J. Liu, S. Vazquez, and S. K. Mazumder, "Sliding Mode Control in Power Converters and Drives: A Review," *IEEE/CAA Journal of Automatica Sinica* 9, no. 3 (March 2022): 392–406, https://doi.org/10.1109/JAS.2021.1004380.

16. A. Govindharaj, A. Mariappan, A. Ambikapathy, V. S. Bhadoria, and H. H. Alhelou, "Real-Time Implementation of Adaptive Neuro Backstepping Controller for Maximum Power Point Tracking in Photo Voltaic Systems," *IEEE Access* 9 (2021): 105859–105875, https://doi.org/10.1109/ACCESS.2021.3099158.

17. P. D. Christofides, J. Liu, and D. Muñoz de la Peña, "Lyapunov-Based Model Predictive Control," in *Networked and Distributed Predictive Control: Methods and Nonlinear Process Network Applications*, ed. P. D. Christofides, J. Liu, and D. Muñoz de la Peña (Springer, 2011), 13–45, https://doi.org/10.1007/978-0-85729-582-8_2.

18. P. Gong, Z. Yan, W. Zhang, and J. Tang, "Lyapunov-Based Model Predictive Control Trajectory Tracking for an Autonomous Underwater Vehicle With External Disturbances," *Ocean Engineering* 232 (July 2021): 109010, https://doi.org/10.1016/j.oceaneng.2021.109010.

19. Q.-C. Zhong and T. Hornik, *Control of Power Inverters in Renewable Energy and Smart Grid Integration* (John Wiley & Sons, 2012), https://doi.org/10.1002/9781118481806.

20. A. S. Soliman, S. M. S. H. Rafin, and O. A. Mohammad, "Enhanced DC Voltage and Power Regulation Using Intelligent Data-Driven Control for AC/DC Converters in DC Microgrid Applications," *IEEE Transactions on Industry Applications* 60, no. 6 (November 2024): 8383–8392, https://doi.org/10.1109/TIA.2024.3429455.

21. M. A. Hannan, Z. Abd Ghani, M. M. Hoque, P. J. Ker, A. Hussain, and A. Mohamed, "Fuzzy Logic Inverter Controller in Photovoltaic Applications: Issues and Recommendations," *IEEE Access* 7 (2019): 24934–24955, https://doi.org/10.1109/ACCESS.2019.2899610.

22. Y. Zhu, Z. Ma, and Z. Wang, "An Improved Fuzzy Logic Based DC-Link Voltage Control Strategy for Smoothing Output Power of the PMSG-WECS," *Energy Reports* 8 (November 2022): 8413–8425, https://doi.org/10.1016/j.egyr.2022.06.049.

23. L. Zhang, Y. Sun, A. Wang, and J. Zhang, "Neural Network Modeling and Dynamic Behavior Prediction of Nonlinear Dynamic Systems," *Nonlinear Dynamics* 111, no. 12 (June 2023): 11335–11356, https://doi.org/10.1007/s11071-023-08407-9.

24. D. Karaboga and E. Kaya, "Adaptive Network Based Fuzzy Inference System (ANFIS) Training Approaches: A Comprehensive Survey," *Artificial Intelligence Review* 52, no. 4 (December 2019): 2263–2293, https://doi.org/10.1007/s10462-017-9610-2.

25. A. Ambroziak and A. Chojecki, "The PID Controller Optimisation Module Using Fuzzy Self-Tuning PSO for Air Handling Unit in Continuous Operation," *Engineering Applications of Artificial Intelligence* 117 (January 2023): 105485, https://doi.org/10.1016/j.engappai.2022.105485.

26. M. F. Hanif, R. Ahmad, A. B. Farooq et al., "The Solar AI Nexus: Reinforcement Learning Shaping the Future of Energy Management," *WIREs Energy and Environment* 14, no. 3 (2025): e70012, https://doi.org/10.1002/wene.70012.

27. A. Behnood, V. Behnood, M. Modiri Gharehveran, and K. E. Alyamac, "Prediction of the Compressive Strength of Normal and High-Performance Concretes Using M5P Model Tree Algorithm," *Construction and Building Materials* 142 (July 2017): 199–207, https://doi.org/10.1016/j.conbuildmat.2017.03.061.

28. M. Mujammal, A. Moualdia, and D. Boudana, "Improved Classic Direct Torque Control Based on Doubly Fed Induction Generator Use Neural Network," in *2021 18th International Multi-Conference on Systems, Signals & Devices (SSD)*, March 2021, 563–568, https://doi.org/10.1109/SSD52085.2021.9429515.

29. R. Kumar Vinod and S. K. Singh, "Solar Photovoltaic Modeling and Simulation: As a Renewable Energy Solution," *Energy Reports* 4 (November 2018): 701–712, https://doi.org/10.1016/j.egyr.2018.09.008.

30. M. A. H. Mujammal, A. Moualdia, S. Boulkhrachef, M. A. Albasheri, and P. Wira, "Implementation of Smart MPPT Strategy Based on Fuzzy Logic Controller for Stand-Alone PV System," in *Technological and Innovative Progress in Renewable Energy Systems: Proceedings of the 2024 International Renewable Energy Days (IREN Days'2024)*, ed. O. Guerri, A. H. Arab, and K. Imessad (Springer Nature, 2025): 55–59, https://doi.org/10.1007/978-3-031-71926-4_9.

31. M. A. H. Mujammal, A. Moualdia, O. Bouchhida, and M. A. Albasheri, "Upgrade Perturbation and Observation of MPPT Strategy via Fuzzy Logic Controller," in *2023 2nd International Conference on Electronics, Energy and Measurement (IC2EM)*, November 2023, 1–7, https://doi.org/10.1109/IC2EM59347.2023.10419670.

32. M. A. H. Mujammal, A. Moualdia, S. Boulkhrachef, D. Boudana, P. Wira, and M. A. Albasheri, "Next-Generation MPPT: Neural Network-Driven Optimization for Superior Solar Performance," *Studies in Engineering and Exact Sciences* 5, no. 2 (September 2024): e7338–e7338, 10.54021/seesv5n2-150.

33. M. A. H. Mujammal, A. Moualdia, P. Wira, M. A. Albasheri, and A. Cherifi, "Novel Direct Power Control Based on Grid Voltage Modulated Strategy Using Artificial Intelligence," *Smart Grids and Energy* 9, no. 2 (October 2024): 37, https://doi.org/10.1007/s40866-024-00225-1.

34. "Microsatellite Yaw-Axis Attitude Control System Using Model Reference Adaptive Control Based PID Controller," *International Journal of Electrical and Computer Engineering Research*, accessed July 18, 2024, https://www.ijecer.org/ijecer/article/view/389.

35. M. Merai, M. W. Naouar, I. Slama-Belkhodja, and E. Monmasson, "An Adaptive PI Controller Design for DC-Link Voltage Control of Single-Phase Grid-Connected Converters," *IEEE Transactions on Industrial Electronics* 66, no. 8 (August 2019): 6241–6249, https://doi.org/10.1109/TIE.2018.2871796.

36. M. A. H. Mujammal, A. Almakki, G. Lorenzini, M. Albasheri, and A. Moualdia, "Optimizing Solar Power: Advanced Maximum Power Point Tracking via Fuzzy Logic for Enhanced Performance and Efficiency," *Indian Journal of Engineering* 22 (August 2025): 10–1686, https://doi.org/10.54905/disssi.v22i58.e10ije1686.

37. M. A. Albasheri, Y. Soufi, O. Bouchhida, M. A. Hasan, A. Cherifi, and S. Khechafi, "Design, Assessment and Implementation of Fuzzy Logic for DC Voltage in Microgrid," in *2025 IEEE 22nd International Multi-Conference on Systems, Signals & Devices (SSD)*, February 2025, 1259–1264, https://doi.org/10.1109/SSD64182.2025.10989848.

38. M. A. Albasheri, O. Bouchhida, Y. Soufi, and A. Cherifi, "Enhanced Vector Control of Induction Motor by Fuzzy Logic Controller," in *2024 2nd International Conference on Electrical Engineering and Automatic Control (ICEEAC)*, May 2024, 1–5, https://doi.org/10.1109/ICEEAC61226.2024.10576217.

39. M. A. Albasheri, O. Bouchhida, Y. Soufi, A. Cherifi, and M. A. H. Mujammal, "Supervisory Energy Management Strategy Based-Fuzzy Logic for a DC Microgrid," *International Journal of Dynamics and Control* 13, no. 1 (January 2025): 31, https://doi.org/10.1007/s40435-024-01510-8.

40. Y. A. Ali, E. M. Awwad, M. Al-Razgan, and A. Maarouf, "Hyperparameter Search for Machine Learning Algorithms for Optimizing the Computational Complexity," *Processes* 11, no. 2 (January 2023), https://doi.org/10.3390/pr11020349.

41. M. A. H. Mujammal, A. Moualdia, S. Boulkhrachef, P. Wira, D. Boudana, and M. A. Albasheri, "Advancing Wind Energy Conversion: Smart Maximum Power Point Based on M5-Pruned Algorithm for Enhanced Wind Energy Production," *Production Engineering – Research and Development* 19, no. 2 (April 2025): 347–368, https://doi.org/10.1007/s11740-024-01315-w.

42. Y. Alsultanny, "Machine Learning by Data Mining REPTree and M5P for Predicating Novel Information for PM_{10}," *Cloud Computing and Data Science* (July 2020): 45–55, https://doi.org/10.37256/ccds.112020418.

43. K. Hornik, C. Buchta, and A. Zeileis, "Open-Source Machine Learning: R Meets Weka," *Computational Statistics* 24, no. 2 (May 2009): 225–232, https://doi.org/10.1007/s00180-008-0119-7.

44. M. Hall, E. Frank, G. Holmes, B. Pfahringer, P. Reutemann, and I. H. Witten, "The WEKA Data Mining Software: An Update," *SIGKDD Explorations Newsletter* 11, no. 1 (November 2009): 10–18, https://doi.org/10.1145/1656274.1656278.